

Article

Impact of Water Content on the Superlubricity of Ethylene Glycol Solutions

Lvzhou Li ^{1,2}, Peng Gong ¹, Pengpeng Bai ², Xiangli Wen ^{1,2}, Yonggang Meng ² , Jianning Ding ¹ and Yu Tian ^{2,*} 

¹ Institute of Technology for Carbon Neutralization, Yangzhou University, Yangzhou 225127, China; 17864225307@163.com (P.G.)

² State Key Laboratory of Tribology, Department of Mechanical Engineering, Tsinghua University, Beijing 100084, China

* Correspondence: tianyu@mail.tsinghua.edu.cn

Abstract: Aqueous solutions of water and ethylene glycol (EG) are prevalently employed in braking, heat transfer, and lubrication systems. However, the precise mechanism through which water content affects the lubricative attributes of EG solutions remains elusive. This research systematically examines the tribological characteristics of EG solutions at varying concentrations using a ceramic–TiAlN friction-pair system. As the concentration of EG increases, the sequential transformation of the associated molecular complex structure in the lubricating medium can be described as follows: $[H_2O]_m \cdot EG \rightarrow [H_2O]_m \cdot [EG]_n \rightarrow H_2O \cdot [EG]_n$. Among them, the stoichiometric coefficients “m” and “n” are the simplest mole ratio of H₂O and EG in the molecular complex structure, respectively. The most favorable EG concentration was determined to be 50 wt.%. At this concentration, a flexible molecular complex adsorption structure ($[H_2O]_m \cdot [EG]_n$) with a significant bearing capacity (due to intense hydrogen bonding) forms on the surface of the friction pair, which results in a reduction in the running-in duration and facilitates the achievement of superlubricity, and the coefficient of friction (COF) is about 0.0047. Solutions containing 50 wt.% EG enhance the load-bearing ability and hydrophilicity of the lubricating medium. Moreover, they minimize the roughness of the worn region and curtail the adhesive forces and shear stress at the frictional interface, enabling the realization of superlubricity. Consequently, this research offers valuable insights into the optimal water-to-EG ratio, revealing the mechanism of a superlubricity system that possesses exceptional tribological attributes and holds significant potential for practical applications.



Citation: Li, L.; Gong, P.; Bai, P.; Wen, X.; Meng, Y.; Ding, J.; Tian, Y. Impact of Water Content on the Superlubricity of Ethylene Glycol Solutions. *Lubricants* **2023**, *11*, 466. <https://doi.org/10.3390/lubricants11110466>

Received: 13 September 2023

Revised: 19 October 2023

Accepted: 23 October 2023

Published: 31 October 2023



Copyright: © 2023 by the authors. Licensee MDPI, Basel, Switzerland. This article is an open access article distributed under the terms and conditions of the Creative Commons Attribution (CC BY) license (<https://creativecommons.org/licenses/by/4.0/>).

Keywords: water–ethylene glycol; optimal ratio; strong hydrogen bonding; $[H_2O]_m \cdot [EG]_n$ -associated structure; superlubricity

1. Introduction

Ethylene glycol (EG) holds the distinction of being the most rudimentary alcohol, excluding polyethylene glycol [1]. It is a prominent ingredient in skin care products [2], antifreezes [3,4], and braking [5,6] and heat transfer systems [7–9], owing to its environmentally friendly nature, efficient heat transfer capabilities, compatibility with various materials, and economical pricing. Over recent decades, a concerted effort has been made to probe the lubricative properties of alcohol-based aqueous solutions, particularly in investigating the feasibility of attaining exceedingly low friction coefficients of below 0.01 [10–12]. Such aqueous solutions, inclusive of alcohol-based polymers and organic acids, promote strong hydrogen bond interactions, consequently accelerating tribochemical reactions and stabilizing the adsorption layer structure on the surface of the friction pair [13,14]. The solutions facilitate the confinement of free water molecules within the contact zone, which augments the system’s load-bearing capacity by reducing the shearing effects at the friction-pair interface. Additionally, hydrated cations adhere strongly to negatively charged ceramic surfaces, resulting in a stable hydrated ion adsorption layer. Hydration and hydrodynamic

lubrication can be used to reduce the initial operational period for lubricating media containing -OH groups, facilitating the achievement of superlubricity under a wide range of experimental conditions [15]. Furthermore, the presence of an alcohol-containing lubricating medium induces the formation of a thicker, denser adsorption layer as elongated alkyl chains accumulate on the bearing steel surface, which, in turn, promotes the formation of a friction-reactive film on the metallic surface. This phenomenon leads to the successful manifestation of macro-superlubricity with alcohol-based aqueous solutions at the bearing steel interface, effectively expanding the applicability scope of the friction-pair system [16]. Current investigations predominantly concentrate on alcohol-based ternary systems to realize reduced friction through synergistic actions, leaving a gap in the research on the lubricative performance of binary systems, such as water-EG solutions.

EG and water molecules can be mixed in any proportion, and with the increase in EG concentration, the -OH stretching vibration peak in water-EG shifts to a low frequency, which effectively reveals the strong hydrogen bond interactions between hydroxyl oxygen atoms in the EG solution [17]. Notably, the water content exerts a profound influence on various aspects, including water activity [18,19], thermal behavior [20], and hydrogen bond strength [21], within the water-alcohol solution. Furthermore, it can affect the utility of the water-alcohol solution as a solvent in catalytic reactions [22], hydrothermal synthesis [23], forced convection heat transfer [24], and the running-in processes of mechanical equipment components [25]. Theoretical calculations have substantiated the presence of an O-C-C-O dihedral structure in the EG molecule within the water-EG solution, corresponding to gauche conformations [21]. By increasing the concentration, the hydrogen bond interactions between EG molecules become more pronounced, reaching an optimal ratio within the water-EG solution system [26]. Experimental evidence also confirms the formation of a novel hydrogen bond network at specific proportions in the water-EG system. As the EG concentration increases, the hydrogen bonds within water molecules first strengthen and subsequently weaken [27,28]. Consequently, the dominant association structure in the water-EG solution transitions from H₂O-H₂O to EG-H₂O. Owing to the robust hydrogen bond interactions and pressure-viscosity effect of water-glycol solutions compared to pure water solvents, when the glycol content exceeds 10%, significant reductions in running-in time and reduced wear can be achieved [25]. It has been found that the viscosity of an EG aqueous solution is a function of EG concentration. Due to the viscosity enhancement and pressure-viscosity effect, an EG aqueous solution can greatly improve the load-carrying capacity, especially in high-concentration solutions, and its wear resistance is significantly improved [25]. In addition, the tribological properties of surfaces with PLL-g-PEG sliding in aqueous glycerol or ethylene glycol solutions under different lubrication regimes were studied, and it was found that the combination of polymer layers on surfaces with aqueous phases of enhanced viscosity greatly reduced the friction [29]. Although some research has been conducted on the physical and chemical properties as well as practical applications of water-glycol systems with varying proportions, the current body of work falls short of elucidating the underlying mechanism influencing the optimal proportion for achieving macro-superlubricity performance in conjunction with water content.

Hence, in this study, we delved into the lubrication performance of aqueous EG solutions with varying concentrations within the Si₃N₄-TiAlN system. Notably, in a 50 wt.% EG aqueous solution, significant reductions in running-in time and the attainment of macro-superlubricity were achieved. These outcomes can be attributed to the formation of a robust hydrogen bond network structure, denoted as [H₂O]_m·[EG]_n, in the 50 wt.% EG aqueous solution. This structure enhances the wetting performance and bearing capacity of the lubricating medium while reducing adhesion and shear stress at the friction-pair interface. Under this specific ratio, the solid-liquid coupling effect exhibited its optimal performance. We conducted an exhaustive and comprehensive experimental investigation of the water-glycol system, analyzing and discussing its running-in process and superlubricity mechanism in detail. This research opens up the possibility of utilizing EG aqueous solutions to achieve ultralow friction in mechanical equipment components.

2. Materials and Methods

2.1. Experimental Materials

For the experiments, the Dow EG solution, with a purity exceeding 99.9%, was procured from Shanghai Kangmiao Trading Co., Ltd. (Shanghai, Beijing). Additionally, high-purity solvents, including petroleum ether, acetone, and absolute ethanol, were obtained from Shanghai Aladdin Biochemical Technology Co., Ltd. (Shanghai, Beijing), with purities surpassing 99%, conforming to international standards [30]. The ultrapure water (UP) utilized in the study exhibited a conductivity of 18.2 M Ω -cm and a total organic carbon content of less than 2 ppb [31]. The friction pair utilized in the experiments comprised a Si₃N₄ ball with a diameter of 3.969 mm (roughness: S_a \approx 4 nm) and a TiAlN disc measuring 24 mm in diameter and 7.88 mm in thickness (S_a < 20 nm) (Figure 1a). The base of the TiAlN disc consisted of 4Cr13 steel, with a uniform TiAlN coating on its surface measuring approximately 2.3 μ m in thickness. The Vickers hardness of the TiAlN coating was approximately 847, representing a 40% increase compared to that of the base steel (Figure 1b). The SiO₂ spherical probe for the atomic force microscope (AFM) consisted of SiO₂ particles with a radius of 20 μ m affixed to the rectangular tip cantilever end using epoxy resin glue. The elastic modulus and Poisson's ratio of the SiO₂ particles were determined to be 50 GPa and 0.17, respectively [32].

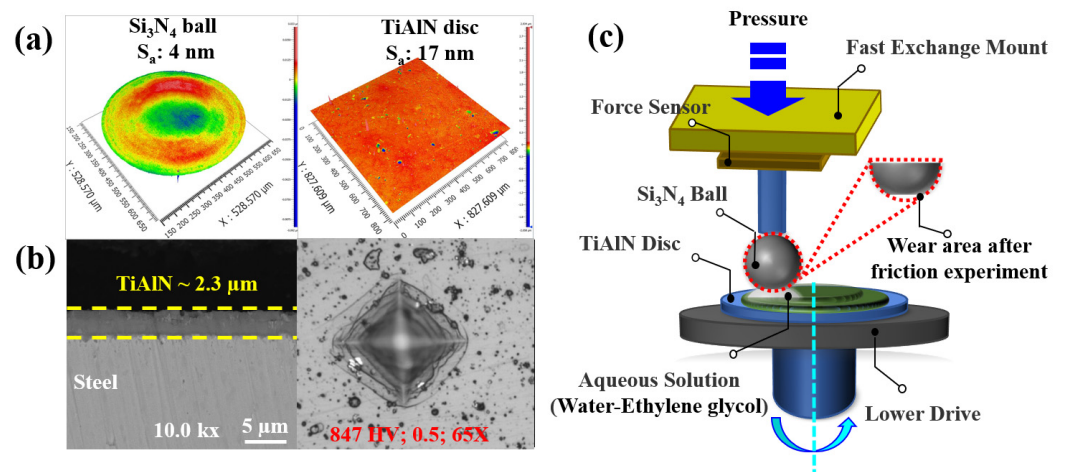


Figure 1. (a) S_a of Si₃N₄ balls and TiAlN discs; (b) cross-section microstructure and surface hardness of TiAlN coating; and (c) schematic diagram of point contact friction and wear experimental equipment.

2.2. Experimental Methods

The point contact friction and wear experiments were conducted in the rotating mode using a multifunctional friction and a wear tester (UMT-5; Bruker, Germany), as illustrated in Figure 1c. Prior to the experiments, both the Si₃N₄ ball and TiAlN disc underwent a thorough cleaning process involving sequential treatments with petroleum ether, acetone, absolute ethanol, and ultrapure water, each lasting for 15 min. Subsequently, they were soaked in absolute ethanol for later use. Before commencing the experiments, the normal and tangential forces of the two-dimensional force sensor (DFM-0.5 kg) were calibrated. A pipette was used to dispense 100 μ L of the lubricating medium between the ball and the disc. The test conditions for evaluating the lubrication performance of water-EG solutions with varying concentrations were as follows: a normal load of 3 N, a rotation radius of 5 mm, and a rotation speed of 180 rpm, corresponding to a linear speed of 94.2 mm/s. All experiments were conducted under ambient conditions of 30 $^{\circ}$ C and 50% humidity. To ensure the reliability of the results, each set of experiments was repeated more than three times.

Both before and after the friction experiments, the surface morphology and wear area of the friction pair were examined using an optical microscope (VHX6000). Furthermore, the surface parameters and micromorphology of the worn areas were characterized using

a three-dimensional white-light interference profilometer (Zygo New View 8300, USA, Connecticut) and a scanning electron microscope (SEM; Quanta 200 FEG, FEI, USA, Massachusetts). The viscosity [33] and wettability of the EG aqueous solutions with varying concentrations were assessed using an Anton Paar rotational rheometer (MCR302) and a video optical contact angle-measuring instrument (Dataphysics OCA 25, Germany, Filderstadt), respectively. Raman spectroscopy (Evolution, HORIBA, France) was employed to collect spectra within the $700\text{--}4000\text{ cm}^{-1}$ range, utilizing a 532 nm laser to discern hydrogen bonding interactions in EG aqueous solutions with different concentrations. Force curves were obtained using an AFM (Dimension ICON, Bruker).

3. Results and Discussion

3.1. Results

Figure 2 depicts the relationship between the coefficients of friction (COFs) of UP and EG over time, obtained under the specified experimental conditions (3 N, 94.2 mm/s, 3600 s). Evidently, UP exhibits poor lubrication performance, with an average COF of 0.1498. During the experiment, the COF exhibited significant fluctuations, primarily attributable to the limited load-carrying capacity of the UP. EG demonstrated superior lubrication performance compared to UP, with the COF gradually decreasing and eventually stabilizing at 0.0226. This improvement is likely linked to the effective adsorption of EG on the surface of the friction pair. Consequently, speculating that the lubrication performance of UP and EG could be enhanced when combined is reasonable. Table 1 provides essential physicochemical parameters for EG solutions with varying concentrations [34,35]. Notably, when the EG concentration reaches 50 wt.%, the freezing point can be reduced to $-33.8\text{ }^{\circ}\text{C}$.

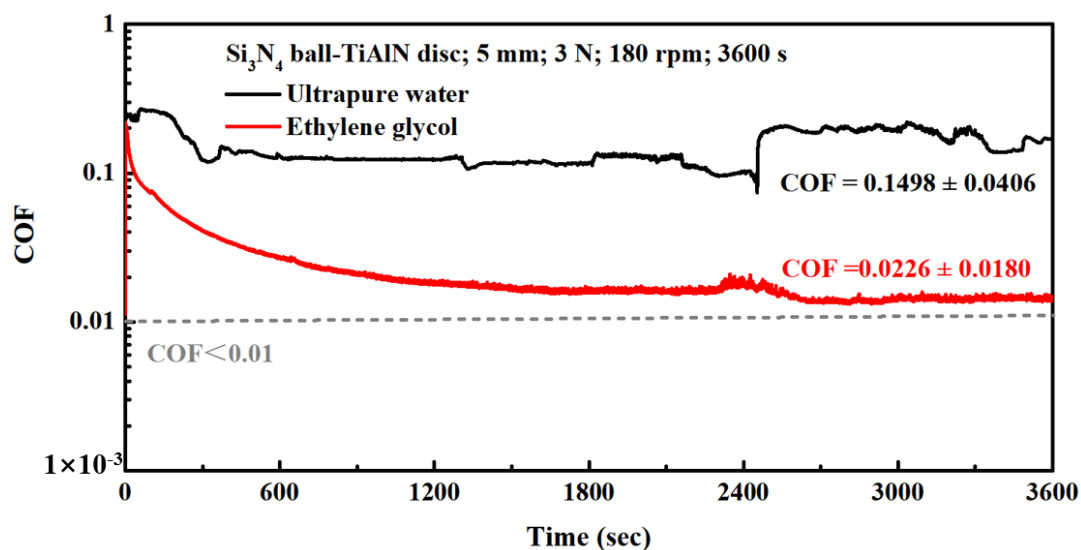
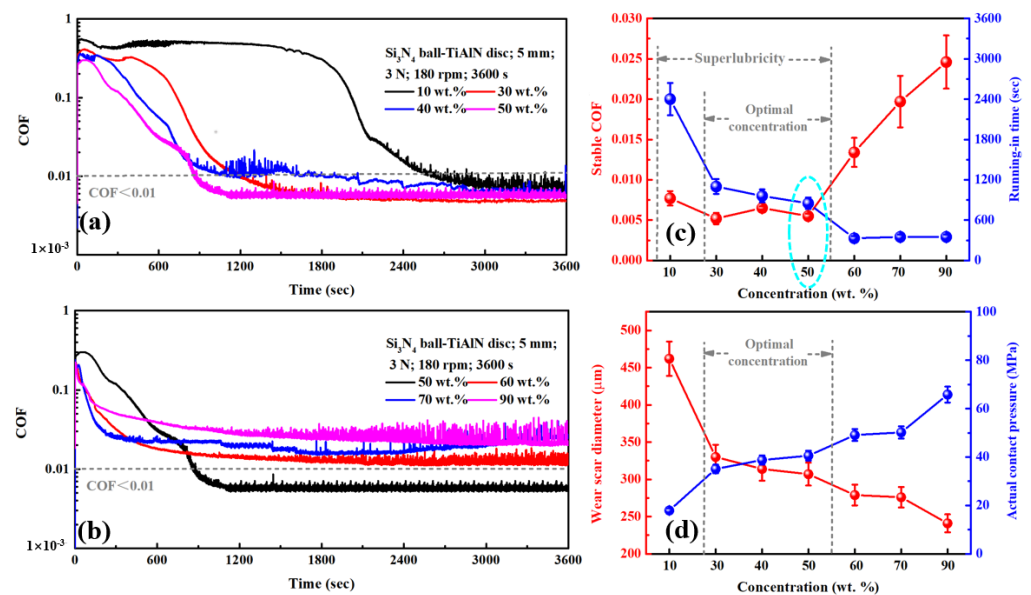


Figure 2. Lubrication performance of UP and EG.

Under identical experimental conditions, the lubrication performances of EG aqueous solutions with different concentrations were further investigated, and the results are displayed in Figure 3. When the EG concentration ranges from 10 to 50 wt.% (Figure 3a), the COF in the initial stage is relatively high, closely resembling that of water in Figure 2. As the friction experiment progresses, an effective running-in process takes place, resulting in a corresponding decrease in COF, ultimately falling below 0.01, signifying the achievement of macro-superlubricity. Conversely, when the EG concentration exceeds 50 wt.% (Figure 3b), the COF rapidly decreases to a stable state, resembling the experimental results of pure EG in Figure 2. During the friction experiment, sporadic “wave peaks” were observed, primarily attributed to abrasive particles generated during the running-in process entering the friction contact area, thereby significantly increasing the instantaneous contact pressure and COF [31].

Table 1. Physicochemical properties of EG aqueous solutions with different concentrations [34,35].

EG Concentration (wt.%)	Freezing Point (°C/°F)	Boiling Point (°C @ 101 kPa/°F @ 760 mmHG)	Degree Brix	Refractive Index 22 °C/72 °F
10	−3.2/26.2	101.1/214	6.8	1.3428
30	−14.1/6.7	104.4/220	19.2	1.3635
40	−22.3/−8.1	105.6/222	25.3	1.3741
50	−33.8/−28.9	107.2/225	31.2	1.3849
60	−48.3/−54.9	110.0/230	36.6	1.3952
70	-/-	116.7/242	41.7	1.4055
90	−29.8/−21.6	140.6/285	51.2	1.4255

**Figure 3.** Friction and wear properties of EG aqueous solutions with different solubility. (a,b) Changes in COF over time; (c) stable COF and running-in time; and (d) wear scar diameter and actual contact pressure of Si₃N₄ balls.

The trends observed for the variations in stable COF/wear scar diameter and running-in time/actual contact pressure in the friction experiments using EG solutions with different concentrations were inversely related (see Figure 3c,d). As the EG concentration increased, the stable COF and actual contact pressure gradually rose, whereas the running-in time and the diameter of wear scars decreased. A comprehensive comparison of these factors led to the determination of the optimal EG concentration range, which was found to be between 30 and 50 wt.%. Within this range, the COF and running-in time were relatively low, and the actual contact pressure could reach approximately 320 MPa. Further analyses revealed that the ideal EG concentration within this range was 50 wt.%. Under this concentration, the running-in time was a mere ~800 s, facilitating the attainment of stable superlubricity with a COF of 0.047. This finding suggests that 50 wt.% EG is highly effective for achieving optimal lubrication performance in the studied system.

The surface parameters of the worn area were meticulously measured and calculated using a three-dimensional white-light topography interferometer, and the results are presented in Figure 4. Figure 4a illustrates the three-dimensional topography of the contact/wear area, with an enlarged view of the blue dotted box on the right, obtained after the friction experiment involving the Si₃N₄ ball and the TiAlN disc. An analysis of the S_a values in the worn areas of both the Si₃N₄ ball and TiAlN disc (Figure 4b) reveals that, as the EG concentration increased, both the S_a of the ball and disc initially decreased before rising. Notably, at an EG concentration of 50 wt.%, the S_a values of both the ball and disc

were minimized. This observation suggests that the running-in process in the early stages of the friction experiment was effective, resulting in minimal wear in the later stages and relatively little change in surface morphology. These factors contribute to the achievement of stable macro-superlubricity.

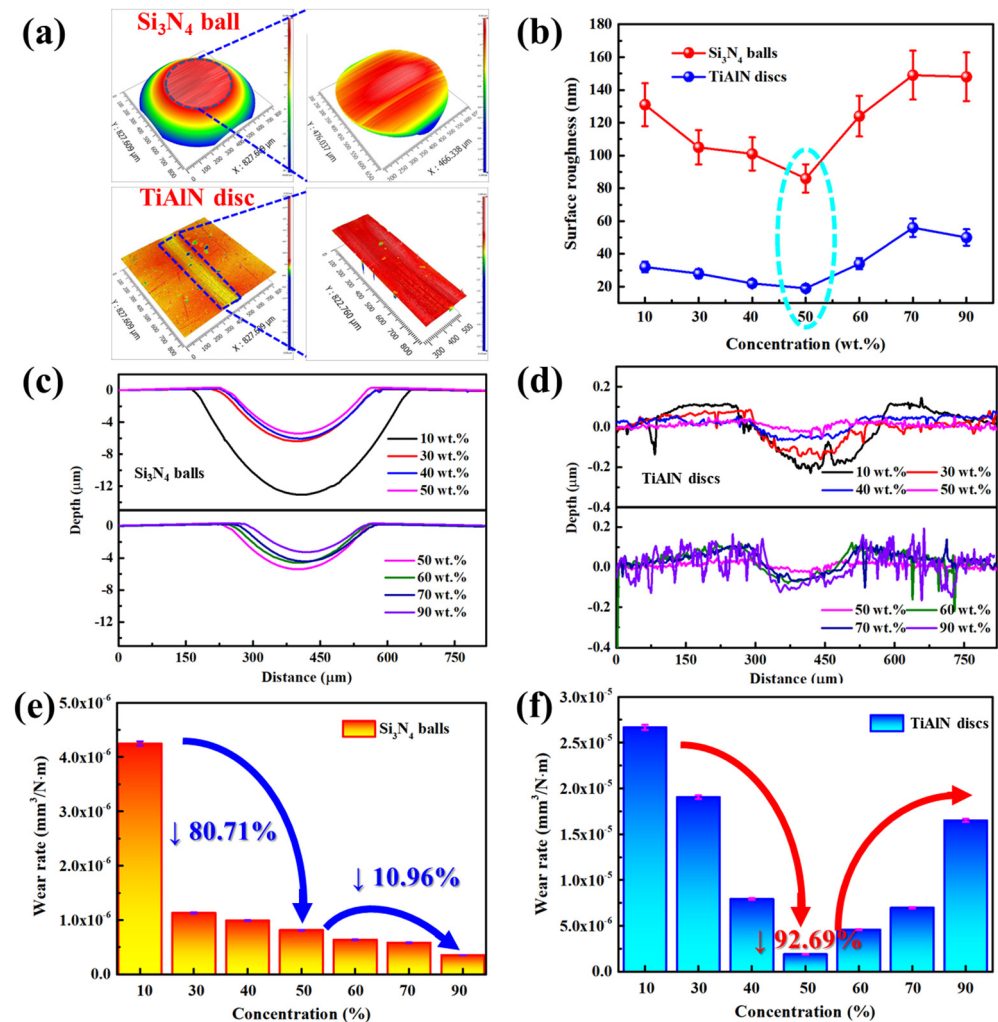


Figure 4. Surface parameters of the worn area of Si₃N₄ balls and TiAlN discs after experiments. (a) 3D white light morphology image and comparison of (b) S_a , (c) wear scar depth, and (d) wear rate results. (e) Wear rates of Wei Si₃N₄ spheres and (f) TiAlN discs at different EG concentrations, respectively.

Additionally, when the EG concentration increased from 10 wt.% to 50 wt.%, the depth of wear marks on the surface of the ball and disc gradually decreased (Figure 4c,d). However, when the concentration reached 90 wt.%, the wear depth exhibited different trends for the ball and disc. The wear depth of the ball progressively decreased with the increase in concentration, whereas the wear depth of the disc increased. This phenomenon can be attributed to the running-in process of the balls. At higher concentrations, the wear spot diameter on the Si₃N₄ ball was smaller, resulting in an increased contact pressure. Furthermore, the hardness of the Si₃N₄ ball exceeded that of the TiAlN disc, exacerbating disc wear. The wear rates of the Si₃N₄ ball and TiAlN disc were also calculated and found to align with the wear depth trends (Figure 4e,f). Specifically, at an EG concentration of 50 wt.%, the wear rate of the ball and disc decreased by 80.71% and 92.69%, respectively, compared to those of the 10 wt.% concentration. When the concentration increased to 90 wt.%, the wear rate of the ball decreased slightly further by 10.96%, whereas the wear rate of the disc exhibited the opposite trend, i.e., it increased.

The above findings underscore the intricate interplay of concentration, wear, and friction performance in this system and emphasize the significant variations in the tribological properties of EG solutions with different concentrations. Consequently, a comprehensive analysis of micromorphology and surface composition was conducted on the worn areas of both the Si_3N_4 ball and TiAlN disc after experiments at different concentrations, as presented in Figure 5. In Figure 5a–d, the surface of the Si_3N_4 ball was initially smooth before the experiment. At an EG concentration of 10 wt.%, noticeable material removal occurred during the experiment, resulting in the formation of furrows and pits caused by wear. When the concentration was increased to 50 wt.%, the surface of the worn area was smooth, with some abrasive particles adhering to it. However, when the concentration was further increased to 90 wt.%, wear became more pronounced, leading to significant material removal and the appearance of a wide range of pits on the surface. An analysis of the composition in the pits and worn areas revealed that a small amount of lubricating medium remained in the pits, leading to a slight increase in the oxygen content. No evident material transfer was observed.

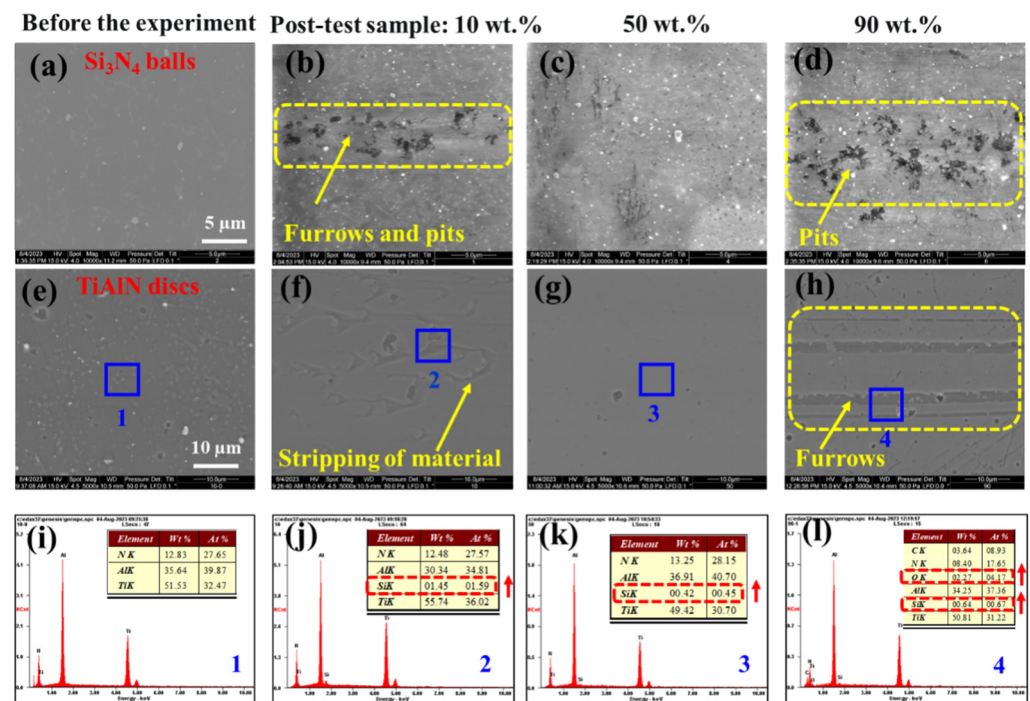


Figure 5. (a–h) Microscopic morphology and (i–l) surface composition analysis of the contact/wear area between (a–d) Si_3N_4 balls and (e–l) TiAlN discs before and after the experiment. Among them, (a,e) are the surface morphology of the (a) Si_3N_4 ball and (e) TiAlN disc, and (i) is the surface composition of the TiAlN disc before the experiment. Surface morphology of (b–d) Si_3N_4 balls and (f–h) TiAlN discs, and (j–l) surface composition of TiAlN discs with (b,f,j) 10 wt.%, (c,g,k) 50 wt.%, and (d,h,l) 90 wt.% of EG solution, respectively, after the friction experiment.

The micromorphology of the contact/wear area on the surface of the TiAlN disc (Figure 5e–h) was initially uniform before the experiment. As the EG concentration increased, the micromorphology of the worn area exhibited the following trend: material peeling due to wear (10 wt.%); slight wear, resulting in a smooth surface (50 wt.%); and severe wear, leading to the formation of numerous deep furrows (90 wt.%). The wear mechanism transitioned from adhesive wear to “two-body” abrasive wear. A surface composition analysis also revealed varying degrees of material transfer in the worn area of the disc. Specifically, the surface silicon element noticeably increased, and the oxygen element within the furrows was relatively abundant (Figure 5i–l). After conducting friction experiments with an EG concentration of 50 wt.%, the surface silicon element increased by

only 0.42 wt.%. This observation supports the notion that wear under this concentration condition was relatively minimal. To sum up, different concentrations of an EG solution will have an important impact on the micro/nano-scale microstructure of the wear region in the friction-pair system. When the concentration of EG is 50 wt.%, the diameter of the wear spot is relatively small, the roughness of the wear area is the lowest, and the surface is relatively smooth, with no obvious wear traces or material transfer.

To ascertain the significant impact of water content on the lubrication performance of the EG solution, a comparative experiment was conducted. In this experiment, 100 μL of a 50 wt.% EG solution was initially applied and operated for 1800 s under the conditions of 3 N and 94.2 mm/s, ensuring complete running-in and the attainment of a superlubricant state (the first stage is shown in Figure 6a). Subsequently, while keeping the contact area of the friction pair unchanged, the worn area was cleaned with absolute ethanol to remove abrasive particles [31] and dried with N_2 to eliminate any residual organic solvent [30]. In the second stage, 100 μL of an EG solution with varying concentrations (10, 50, and 90 wt.%) was introduced into the contact area individually, and the operation continued for 1800 s under the same conditions. The variation in the COF over time is presented in Figure 6b. Notably, the same colors in Figure 6 represent the results of different stages within the same group of comparative experiments.

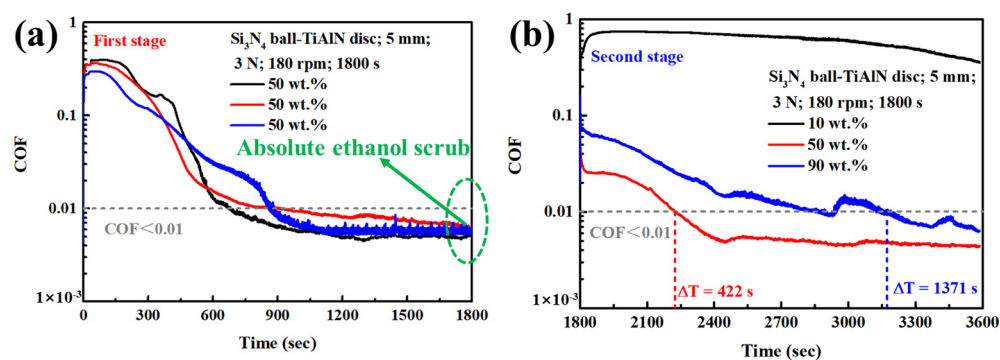


Figure 6. (a) After achieving superlubricity with a 50 wt.% EG aqueous solution, the surfaces of the ball and disc are scrubbed clean. (b) Lubrication performance with the addition of different concentrations of EG aqueous solutions.

The results revealed that the 50 wt.% EG solution exhibited good repeatability. However, when the lubricating medium was reapplied, the 10 wt.% EG aqueous solution displayed a relatively high COF, similar to the initial running-in stage in Figure 3a. Following the initial stage with the 50 wt.% EG aqueous solution (Figure 6a), the 10 wt.% EG aqueous solution still could not achieve superlubricity. This observation might be attributed to the stable adsorption process of molecules at the interface of the friction pair. In the second stage, both the 50 wt.% and 90 wt.% EG aqueous solutions required additional running-in, eventually achieving a COF of less than 0.01. However, the running-in time differed between the two solutions, with the 50 wt.% EG aqueous solution requiring 422 s and the 90 wt.% EG aqueous solution taking 1371 s to achieve superlubricity. These findings emphasize the role of water content in influencing the lubrication performance of the EG solution and highlight the importance of achieving the optimal water–EG concentration for desired tribological outcomes.

The results indicate that absolute ethanol not only removes excess lubricating media and generated abrasive particles but may also impact the molecular adsorption on the surface of the friction pair. When an EG aqueous solution is reapplied, a re-running-in process is necessary to enable the arrangement and combination of the lubricating medium on the surface, forming an effective adsorption layer. This process takes less time (~ 800 s) than it does for the 50 wt.% EG aqueous solution in Figure 3b. In the initial stage, the 50 wt.% EG aqueous solution undergoes running-in to create a larger wear spot diameter, enabling the 90 wt.% EG aqueous solution to achieve macro-superlubricity in the second stage.

These findings underscore the significant influence of water content on the adsorption process and adsorption groups of the EG solution in the wear area, ultimately affecting the lubrication performance of the mixed system.

3.2. Discussion

The viscosity of EG aqueous solutions with varying concentrations and the contact angles (CAs) on the surface of the TiAlN disc were measured, and the results are presented in Figure 7. The viscosity of pure water at room temperature is approximately 0.89 mPa·s [36], and it increases with the EG concentration (Figure 7a). This increase contributes to the formation of a stable lubricating film on the surface of the friction pair, enhancing the load-bearing capacity of the system. Additionally, Figure 7b shows that when the EG concentration is below 10 wt.%, the CA is relatively high ($\sim 86^\circ$). However, as the concentration reached 30 wt.%, the CA stabilized at around 65° , and further concentration increases had a minimal effect on wettability. Specifically, the contact angles for 10, 50, and 90 wt.% EG were 86° , 60° , and 56° , respectively. The transition from 10 to 50 wt.% EG resulted in a 30.23% reduction in the measured CA, effectively improving the spreading ability of the lubricating medium on the surface and providing a foundation for stable molecule adsorption.

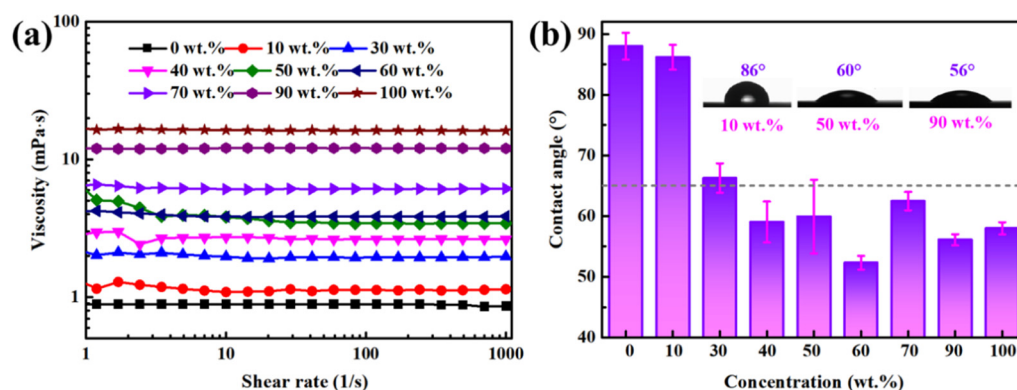


Figure 7. (a) Viscosities [36] of EG aqueous solutions with different concentrations and (b) CA on the surface of TiAlN disc.

To investigate the influence of water content on hydrogen bond strength and the association structure between H_2O and EG, Raman spectra of EG aqueous solutions with varying concentrations in the range of $700\text{--}4000\text{ cm}^{-1}$ were conducted, and the results are displayed in Figure 8a. Figure 8b,c provide enlarged views of the red and blue dotted boxes in Figure 8a, respectively. In the Raman spectrum of pure water, two peaks appear at approximately 3260 and 3458 cm^{-1} , corresponding to the symmetric and asymmetric stretching vibration peaks of O-H, respectively [37,38]. The color-coded markings in Figure 8b illustrate that, as the EG concentration increases, both the symmetric and asymmetric O-H peaks undergo a blue shift (an increase in wave number), followed by a red shift (a decrease in wave number). Notably, at an EG concentration of 50 wt.%, the wavelength of the O-H corresponding peak reached its maximum. The spectrum of EG within the $2800\text{--}3000\text{ cm}^{-1}$ range was further amplified and analyzed (Figure 8c). The peaks at 2891 and 2948 cm^{-1} can also be attributed to the hydrogen bond structure in EG molecules [28]. The color development pattern also reveals that the corresponding Raman peak undergoes significant changes with varying EG concentrations. As the EG concentration increases, the O-H Raman peak follows a similar trend to that observed in H_2O , initially shifting toward the blue and then toward the red. At the 50 wt.% EG concentration, the wavelength corresponding to the Raman characteristic peak of hydrogen bonding reaches its maximum. These findings indicate that as the EG concentration increases, the hydrogen bonds within H_2O molecules undergo alterations, leading to changes in the molecular association structure between H_2O and EG. In an aqueous EG solution, EG exists as a mixture of trans and gauche conformations [27]. However, due to intramolecular hydrogen

bonding (dipole–dipole interactions), the gauche conformation predominates and is more stable than the trans conformation.

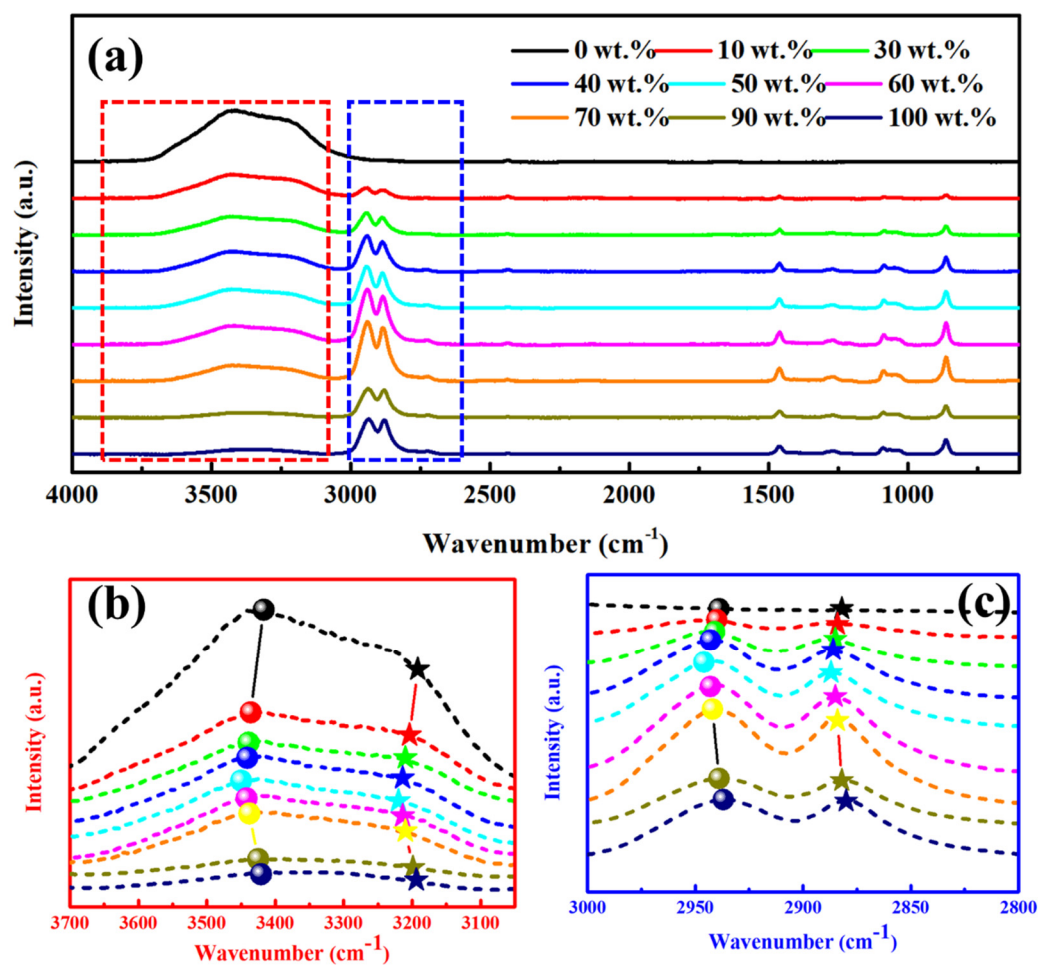


Figure 8. (a) Raman spectra of different concentrations of EG aqueous solutions and (b,c) enlarged images of local regions.

This phenomenon occurs because the interaction between EG and H₂O is more favorable than that between H₂O and H₂O. At lower EG concentrations, EG molecules form hydrogen bonds with adjacent H₂O molecules through -OH groups. Excess water molecules surround the EG, resulting in the formation of water clusters around the -OH groups of the EG. As the EG concentration increases, these water clusters gradually become smaller [39]. Consequently, at lower concentrations, the primary structure formed is [H₂O]_m·EG, leading to a relatively low O-H Raman peak for water. However, when the EG concentration reaches 50 wt.%, the abundance of -OH groups in EG enables it to act simultaneously as a proton donor and acceptor, effectively interacting with H₂O [40]. This interaction disrupts the hydrogen bond structure in H₂O, causing the O-H Raman peak to shift to a higher wave number. At this point, the primary form of the association structure in the solution becomes [H₂O]_m·[EG]_n. This structure consists of interconnected H₂O and EG molecules through a hydrogen bonding network, forming closed or open annular planes with strong rigidity capable of bearing significant loads. As the EG concentration increases further, a small number of H₂O molecules disperse as monomers. These monomers take precedence over the hydrophilic groups of EG clusters for hydrogen bonding associations, resulting in a structure of H₂O·[EG]_n. The association structures of H₂O and EG differ with changes in EG concentration, leading to variations in the strength of the hydrogen bonds formed between them.

Subsequently, the force curves and statistical results of the adhesion of EG aqueous solutions with different concentrations on the surfaces of monocrystalline silicon wafers and TiAlN discs were measured, and the results are depicted in Figure 9. In the figure, the abscissa represents the displacement of the needle tip, whereas the ordinate indicates the magnitude of the interaction force between the needle tip and the surface of the friction pair. The findings reveal that as the EG concentration increases, the adhesion on the surfaces of both the monocrystalline silicon wafer and TiAlN disc follows the same pattern: the adhesion initially decreases and then increases (Figure 9a,b). At a concentration of 50 wt.%, the adhesion force is at its minimum, with adhesion forces of 0.02 nN and 0.24 nN on the surfaces of the monocrystalline silicon wafer and TiAlN disc, respectively. This reduction in adhesion effectively lowers the friction, representing a necessary condition for achieving macro-superlubricity. The statistical results affirm the repeatability of the experiment and indicate an optimal EG aqueous solution ratio of 1:1. This finding aligns with the experimental results for friction and wear (Figure 9c,d) and further supports the efficacy of the 50 wt.% EG aqueous solution in achieving superior lubrication performance.

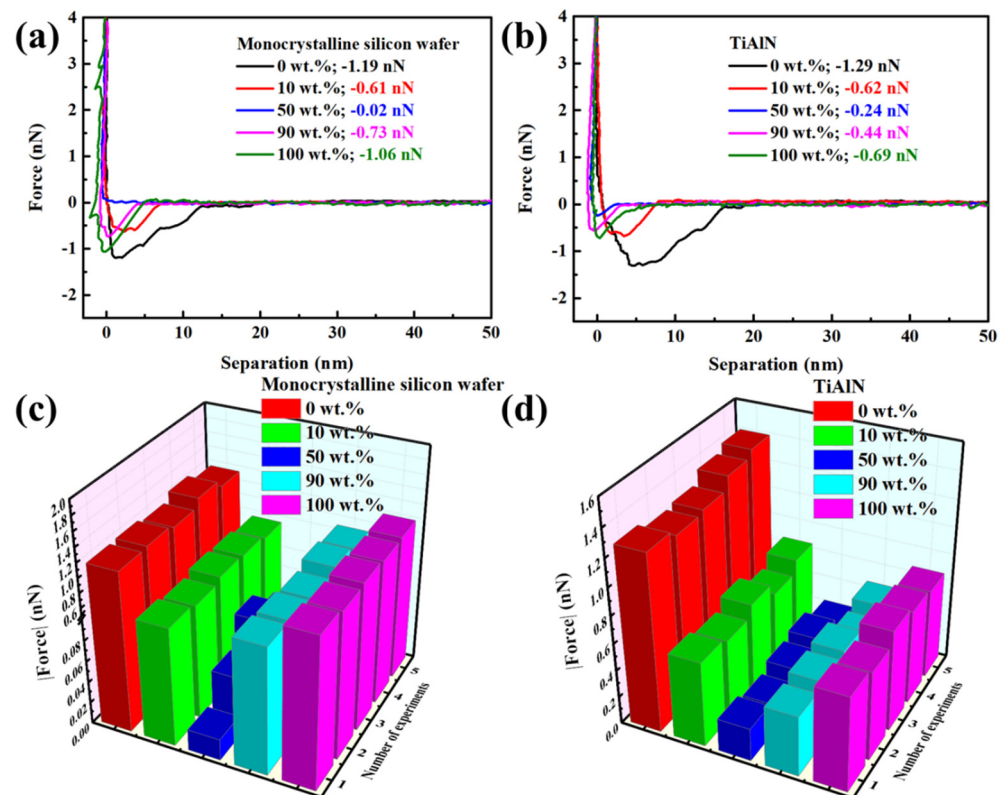


Figure 9. (a,b) Adhesion curves and (c,d) adhesion statistical results of different concentrations of EG aqueous solutions on (a,c) monocrystalline silicon wafers and (b,d) TiAlN discs.

A superlubricity mechanism involving a 50 wt.% EG aqueous solution is illustrated in Figure 10. When the EG concentration was low, the wettability was poor, and the lubricating medium could not adequately cover the worn area. As the EG concentration increased, the running-in time gradually decreased, and the surface S_a of the worn area reached its minimum at a concentration of 50 wt.%. Considering wettability, wear area, and S_a when the amount of the lubricating medium was consistent, a lubricating medium with a 50 wt.% concentration could effectively distribute itself in the contact area, forming a stable and continuous friction adsorption film (Figure 10a,b).

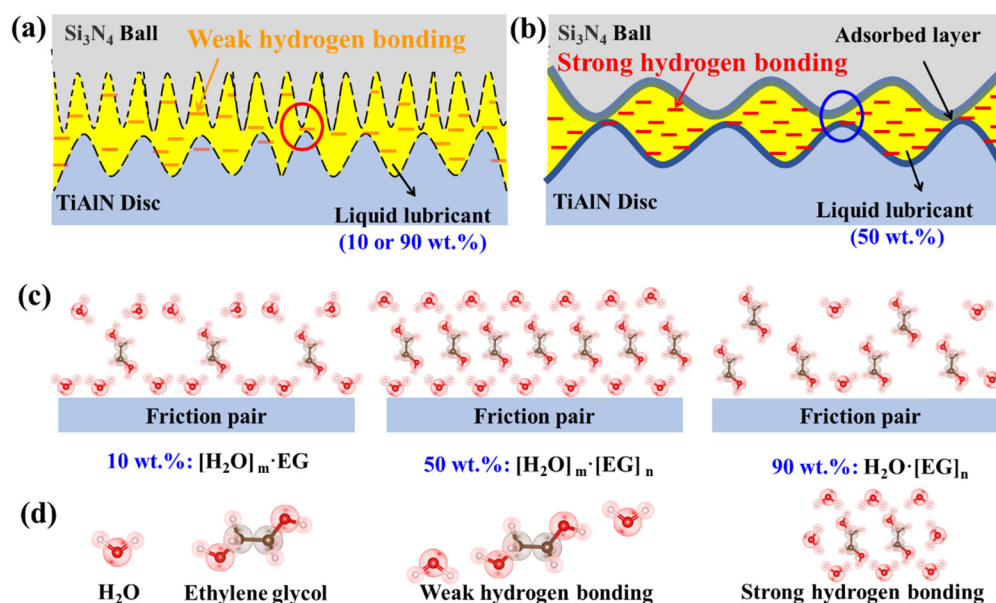


Figure 10. Schematic diagram of the mechanism of achieving superlubricity with a 50 wt.% EG aqueous solution. For different concentrations of EG solution, (a,b) schematic diagram of contact area of friction pair, (c) schematic diagram of adsorption structure of friction pair surface, and (d) schematic diagram of different molecular structure.

When the EG concentration is increased, the transformation process of the association structure in the lubricating medium progresses as follows: $[\text{H}_2\text{O}]_m \cdot \text{EG} \rightarrow [\text{H}_2\text{O}]_m \cdot [\text{EG}]_n \rightarrow \text{H}_2\text{O} \cdot [\text{EG}]_n$ (Figure 10c). When the concentration reaches 50 wt.%, a closed or open annular planar structure $[\text{H}_2\text{O}]_m \cdot [\text{EG}]_n$ forms by connecting H₂O and EG molecules through a hydrogen bonding network (Figure 10d). It is worth noting that during the whole experiment, a stable, strong hydrogen bond interaction was formed in the 50 wt.% water-EG solution, which ensured that the stable association structure did not change greatly under a certain load and shear force. This structure adheres stably to the contact area of the friction pairs and possesses a high load-bearing capacity. It effectively prevents direct contact between the friction pairs, reduces shear resistance, and facilitates the realization of superlubricity.

4. Conclusions

In this comprehensive study, we systematically explored the tribological properties of EG aqueous solutions with different concentrations and assessed the impact of water content on hydrogen bonding and lubrication performance. Our findings led to several key conclusions.

At a concentration of 50 wt.%, a stable $[\text{H}_2\text{O}]_m \cdot [\text{EG}]_n$ adsorption film formed on the surface of the friction pair. This structure exhibited significant rigidity, effectively preventing direct contact between friction pairs, reducing shear forces, and enabling macro-superlubricity. The progression of association structures in the lubricating medium with increasing EG concentrations follows this sequence: $[\text{H}_2\text{O}]_m \cdot \text{EG} \rightarrow [\text{H}_2\text{O}]_m \cdot [\text{EG}]_n \rightarrow \text{H}_2\text{O} \cdot [\text{EG}]_n$. Additionally, characteristic Raman peaks of O-H in both H₂O and EG shift from blue to red as the EG concentration increases. This shift further supports the evolution of the H₂O-EG association structure. Further, increasing the EG concentration leads to enhanced viscosity and wettability of the lubricating medium. These changes provide prerequisites for reducing the running-in time and achieving superlubricity.

Our systematic exploration of the tribological properties of aqueous EG solutions on ceramic-TiAlN coatings offers a solid foundation for their application in braking and heat transfer systems. It also provides theoretical support for selecting the optimal water-to-EG ratio and opens up possibilities for the broader application of environmentally friendly water-glycol binary superlubricity systems. These findings contribute to our understanding

of lubrication mechanisms and offer practical insights for improving the efficiency and sustainability of various mechanical systems.

Author Contributions: L.L.: Methodology, validation, formal analysis, data curation, writing—review and editing, and writing—original draft. P.G.: experimental operation, validation, and data curation. P.B.: experimental operation, validation, data curation, and writing—review and editing. X.W.: experimental operation, validation, and data curation. Y.M.: conceptualization, validation, formal analysis, and writing—review and editing. J.D.: formal analysis, data curation, and supervision. Y.T.: validation, investigation, formal analysis, supervision, project administration, and funding acquisition. All authors have read and agreed to the published version of the manuscript.

Funding: This work was financially supported by the Tribology Science Fund of the State Key Laboratory of Tribology (No. SKLTKF22A02) and the National Natural Science Foundation of China (Nos. 52175176 and 52275198).

Data Availability Statement: The data presented in this study are available on request from the corresponding author. The data are not publicly available due to confidentiality reasons.

Acknowledgments: The authors are very grateful for the helpful discussions with Luo Yue and Yan Meng.

Conflicts of Interest: The authors declare no conflict of interest.

Abbreviations

EG: ethylene glycol; UP: ultrapure water; S_a : roughness; SEM: scanning electron microscope; AFM: atomic force microscope; COF: coefficient of friction; CA: contact angle.

References

1. Stellman, J.M. *Encyclopaedia of Occupational Health and Safety*; International Labour Organization: Geneva, Switzerland, 1998.
2. Goto, T.; Yin, S.; Sato, T. Morphological control of zinc oxide and application to cosmetics. *Int. J. Nanotechnol.* **2013**, *10*, 48–56. [[CrossRef](#)]
3. Seiler, J.; Hackmann, J.; Lanzerath, F.; Bardow, A. Refrigeration below zero C: Adsorption chillers using water with ethylene glycol as antifreeze. *Int. J. Refrig.* **2017**, *77*, 39–47. [[CrossRef](#)]
4. Nguyen, T.; Zhao, M.; Geng, S.; Ivey, D. Ethylene Glycol as an Antifreeze Additive and Corrosion Inhibitor for Aqueous Zinc-Ion Batteries. *Batter. Supercaps.* **2022**, *5*, e202100420. [[CrossRef](#)]
5. Singh, T.; Jain, M.; Ganguli, D.; Ravi, K. Evaluation of water glycol hydraulic fluids: A tribological approach. *J. Synth. Lubric.* **2006**, *23*, 177–184. [[CrossRef](#)]
6. Wang, J.; Xu, C.; Wang, J.; Li, C.; Zhao, G.; Wang, X. Tribological properties of three S-Alkyl-N, N-dicarboxymethyl dithiocarbamates as additives in water–glycol hydraulic fluid. *Tribol. Trans.* **2013**, *56*, 374–384. [[CrossRef](#)]
7. Peyghambarzadeh, S.; Hashemabadi, S.; Hoseini, S.; Jamnani, M. Experimental study of heat transfer enhancement using water/ethylene glycol based nanofluids as a new coolant for car radiators. *Int. Commun. Heat Mass Transfer* **2011**, *38*, 1283–1290. [[CrossRef](#)]
8. Azmi, W.; Hamid, K.; Usri, N.; Mamat, R.; Sharma, K. Heat transfer augmentation of ethylene glycol: Water nanofluids and applications—A review. *Int. Commun. Heat Mass Transfer* **2016**, *75*, 13–23. [[CrossRef](#)]
9. Soltani, F.; Hajian, M.; Toghraie, D.; Gheisari, A.; Sina, N.; Alizadeh, A. Applying Artificial Neural Networks (ANNs) for prediction of the thermal characteristics of engine oil-based nanofluids containing tungsten oxide-MWCNTs. *Case Stud. Therm. Eng.* **2021**, *26*, 101122. [[CrossRef](#)]
10. Matta, C.; Joly-Pottuz, L.; Bouchet, M.; Martin, J.; Kano, M.; Zhang, Q.; Goddard, W. Superlubricity and tribochemistry of polyhydric alcohols. *Phys. Rev. B* **2008**, *78*, 85436. [[CrossRef](#)]
11. Jia, W.; Tian, J.; Bai, P.; Li, S.; Zeng, H.; Zhang, W.; Tian, Y. A novel comb-typed poly (oligo (ethylene glycol) methylether acrylate) as an excellent aqueous lubricant. *J. Colloid Interface Sci.* **2019**, *539*, 342–350. [[CrossRef](#)]
12. Liu, W.; Wang, H.; Liu, Y.; Zhang, C.; Luo, J. Controllable superlubricity system of polyalkylene glycol aqueous solutions under various applied conditions. *Macromol. Mater. Eng.* **2020**, *305*, 2000141. [[CrossRef](#)]
13. Du, C.; Yu, T.; Wu, Z.; Zhang, L.; Shen, R.; Li, X.; Feng, M.; Feng, Y.; Wang, D. Achieving macroscale superlubricity with ultra-short running-in period by using polyethylene glycol-tannic acid complex green lubricant. *Friction* **2023**, *11*, 748–762. [[CrossRef](#)]
14. Liu, W.; Wang, H.; Liu, Y. Adjustable superlubricity system using polyalkylene glycol with various acid aqueous solutions. *Friction* **2023**, *11*, 1138–1149. [[CrossRef](#)]

15. Han, T.; Yi, S.; Zhang, C.; Li, J.; Chen, X.; Luo, J.; Banquy, X. Superlubrication obtained with mixtures of hydrated ions and polyethylene glycol solutions in the mixed and hydrodynamic lubrication regimes. *J. Colloid Interface Sci.* **2020**, *579*, 479–488. [[CrossRef](#)]
16. Zheng, Z.; Liu, X.; Yu, H.; Chen, H.; Feng, D.; Qian, D. Insight into macroscale superlubricity of polyol aqueous solution induced by protic ionic liquid. *Friction* **2022**, *10*, 2000–2017. [[CrossRef](#)]
17. Zhang, J.; Zhang, P.; Ma, K.; Han, F.; Chen, G.; Wei, X. Hydrogen bonding interactions between ethylene glycol and water: Density, excess molar volume, and spectral study. *Sci. China Ser. B-Chem.* **2008**, *51*, 420–426. [[CrossRef](#)]
18. Ninni, L.; Camargo, M.; Meirelles, A. Water activity in poly (ethylene glycol) aqueous solutions. *Thermochim. Acta* **1999**, *328*, 169–176. [[CrossRef](#)]
19. Gmbh, R. *Automotive Handbook*; Society of Automotive Engineers: Germany, Bosch, 2004.
20. Baudot, A.; Odagescu, V. Thermal properties of ethylene glycol aqueous solutions. *Cryobiology* **2004**, *48*, 283–294. [[CrossRef](#)] [[PubMed](#)]
21. De, O.; Freitas, L. Molecular dynamics simulation of liquid ethylene glycol and its aqueous solution. *J. Mol. Struct.-Theochem.* **2005**, *728*, 179–187.
22. Wang, Y.; Zhao, N.; Fang, B.; Li, H.; Bi, X.; Wang, H. Effect of different solvent ratio (ethylene glycol/water) on the preparation of Pt/C catalyst and its activity toward oxygen reduction reaction. *RSC Adv.* **2015**, *5*, 56570–56577. [[CrossRef](#)]
23. Wojnarowicz, J.; Opalinska, A.; Chudoba, T.; Gierlotka, S.; Mukhovskiy, R.; Pietrzykowska, R.; Sobczak, K.; Lojkowski, W. Effect of water content in ethylene glycol solvent on the size of ZnO nanoparticles prepared using microwave solvothermal synthesis. *J. Nanomater.* **2016**, *2016*, 2789871. [[CrossRef](#)]
24. Azmi, W.; Usri, N.; Mamat, R.; Sharma, K.; Noor, M. Force convection heat transfer of Al₂O₃ nanofluids for different based ratio of water: Ethylene glycol mixture. *Appl. Therm. Eng.* **2017**, *112*, 707–719. [[CrossRef](#)]
25. Yan, S.; Lin, B.; Zhang, X.; Wang, A.; Zhou, X. Investigation of the running-in process of silicon nitride sliding in aqueous solutions of ethylene glycol. *Tribol. Int.* **2015**, *90*, 386–392. [[CrossRef](#)]
26. Weng, L.; Chen, C.; Zuo, J.; Li, W. Molecular dynamics study of effects of temperature and concentration on hydrogen-bond abilities of ethylene glycol and glycerol: Implications for cryopreservation. *J. Phys. Chem. A* **2011**, *115*, 4729–4737. [[CrossRef](#)]
27. Krishnan, K.; Krishnan, R. Raman and Infrared Spectra of Ethylene Glycol. In Proceedings of the Indian Academy of Sciences-Section A; Springer: New Delhi, India, 1966; Volume 64, pp. 111–122.
28. Wang, Y.; Li, F.; Fang, W.; Sun, C.; Men, Z. Study of hydrogen bonding interactions in ethylene glycol-water binary solutions by Raman spectroscopy. *Spectrochim. Acta A* **2021**, *260*, 119916. [[CrossRef](#)] [[PubMed](#)]
29. Nalam, P.; Clasohm, J.; Mashaghi, A.; Spencer, N. Macrotribological Studies of Poly(L-lysine)-graft-Poly(ethylene glycol) in Aqueous Glycerol Mixtures. *Tribol. Lett.* **2009**, *37*, 541–552. [[CrossRef](#)]
30. Wen, X.; Fang, J.; Bai, P.; Li, Y.; Meng, Y.; Ma, L.; Tian, Y. Significantly Affected Lubrication Behavior of Silicone Oil Lubricated Si₃N₄/Glass Contact after Cleaning with Different Solvents. *Langmuir* **2022**, *39*, 155–167. [[CrossRef](#)]
31. Wen, X.; Bai, P.; Li, Y.; Cao, H.; Li, S.; Wang, B.; Fang, J.; Meng, Y.; Ma, T.; Tian, Y. Effects of Abrasive Particles on Liquid Superlubricity and Mechanisms for Their Removal. *Langmuir* **2021**, *37*, 3628–3636. [[CrossRef](#)]
32. Han, T.; Zhang, C.; Chen, X.; Li, J.; Wang, W.; Luo, J. The Contribution of Tribo-Induced Silica Layer to Macroscale Superlubricity of Hydrated Ions. *J. Phys. Chem. C* **2019**, *123*, 20270–20277. [[CrossRef](#)]
33. Wen, X.; Bai, P.; Meng, Y.; Ma, L.; Tian, Y. High-Temperature Superlubricity Realized with Chlorinated-Phenyl and Methyl-Terminated Silicone Oil and Hydrogen-Ion Running-in. *Langmuir* **2022**, *38*, 10043–10051. [[CrossRef](#)]
34. Dye, R. Ethylene glycols technology. *Korean J. Chem. Eng.* **2001**, *18*, 571–579. [[CrossRef](#)]
35. Inhibited Ethylene Glycol-Based Heat Transfer Fluid. Available online: <https://www.dow.com> (accessed on 22 October 2023).
36. Gupta, S. Viscosity of Water. In *Viscometry for Liquids: Calibration of Viscometers*; Springer International Publishing: Cham, Switzerland, 2014; pp. 197–226.
37. Giguère, P. Bifurcated hydrogen bonds in water. *J. Raman Spectrosc.* **1984**, *15*, 354–359. [[CrossRef](#)]
38. Du, Q.; Freysz, E.; Shen, Y. Vibrational spectra of water molecules at quartz/water interfaces. *Phys. Rev. Lett.* **1994**, *72*, 238. [[CrossRef](#)] [[PubMed](#)]
39. Kumar, R.; Baskar, P.; Balamurugan, K.; Das, S.; Subramanian, V. On the perturbation of the H-bonding interaction in ethylene glycol clusters upon hydration. *J. Phys. Chem. A* **2012**, *116*, 4239–4247. [[CrossRef](#)] [[PubMed](#)]
40. Chen, Y.; Ozaki, Y.; Czarniecki, M. Molecular structure and hydrogen bonding in pure liquid ethylene glycol and ethylene glycol–water mixtures studied using NIR spectroscopy. *Phys. Chem. Chem. Phys.* **2013**, *15*, 18694–18701. [[CrossRef](#)] [[PubMed](#)]

Disclaimer/Publisher’s Note: The statements, opinions and data contained in all publications are solely those of the individual author(s) and contributor(s) and not of MDPI and/or the editor(s). MDPI and/or the editor(s) disclaim responsibility for any injury to people or property resulting from any ideas, methods, instructions or products referred to in the content.